XIII International Conference on Computational Plasticity. Fundamentals and Applications
COMPLAS XIII
E. Oñate, D.R.J. Owen, D. Peric and M. Chiumenti (Eds)

REVERSE LOADING TESTS OF STEEL TUBE UNDER BIAXIAL STRESS STATES

DAISAKU YANAGA[†], KOUICHI KURODA[†], SATOSHI YAITA[‡] AND TOSHIHIKO KUWABARA[‡]

[†]R & D Laboratories Nippon Steel & Sumitomo Metal Corporation
1-8 Fuso-cho, Amagasaki-shi, Hyogo, 660-0891, Japan
e-mail: yanaga.2ft.daisaku@jp.nssmc.com

[‡]Division of Advanced Mechanical Systems Engineering,
Institute of Engineering, Tokyo University of Agriculture and Technology
2-24-16, Nakacho, Koganei-shi, Tokyo, 184-8588, Japan

Key words: Biaxial stress, Reverse loading, Yield function, Bauschinger effect

Abstract. Biaxial loading and reverse loading tests were performed using seamless carbon steel tubes. Biaxial stress components in the axial and circumferential directions were applied to the tubular specimens using a servo-controlled multiaxial tube expansion testing machine developed by Kuwabara and Sugawara (2013). The tubular specimens were loaded under linear tensile stress paths. Contours of plastic work were measured in the principal stress space, and the differential hardening (DH) behavior was observed; the shapes of the contours of plastic work changed with an increase in plastic work. In addition, small uniaxial tensile specimens were fabricated from the mother tube wall in axial and hoop directions, and tension–compression reverse loading tests were performed to quantitatively evaluate the Bauschinger effect of the test material. Moreover, bilinear stress path experiments were performed to investigate the effects of axial prestraining on the change in the Bauschinger effect; compressive preloading in the axial direction (first loading) was followed by the application of linear stress paths in the first quadrant of the principal stress space (second loading). The measured Bauschinger effect in the second loading was different from those measured in the uniaxial reverse loading tests for the as-received material. The material model will be utilized to improve the accuracy in the numerical analyses of the cold working processes for fabricating steel tubes.

1 INTRODUCTION

In recent years, the deformation behavior of materials in metal forming processes is predicted using finite element analyses (FEA). In case of cold working simulations of steel tube processing, an isotropic yield function [1], associated flow rule, and isotropic hardening are assumed as a material model, as shown in equations (1–3).

$$\phi_M^2 = \frac{3}{2}\boldsymbol{\sigma}' : \boldsymbol{\sigma}' \tag{1}$$

$$d\boldsymbol{\varepsilon}^{\mathrm{p}} = \gamma \frac{\partial f}{\partial \boldsymbol{\sigma}} \tag{2}$$

$$W^{\mathrm{p}} = \int \bar{\sigma} d\bar{\varepsilon}^{\mathrm{p}} = \int \boldsymbol{\sigma} d\boldsymbol{\varepsilon}^{\mathrm{p}} \tag{3}$$

$\boldsymbol{\sigma}'$: Deviatoric stress

ϕ_M : von Mies yield function

f : Yield condition

γ : Plastic mulitplier

W^p : Total plastic work

$\bar{\sigma}$: Equivalent stress

$\bar{\varepsilon}^{\mathrm{p}}$: Equivalent strain

Using these models, plastic material parameter is prepared on the basis of equivalent stress–strain relationship. Usually, that is measured by uniaxial tension test. However, such models cannot reproduce actual phenomena obtained from detailed observation of actual plastic deformation behavior such as initial and subsequent anisotropy and Bauschinger effect. To improve the predictive accuracy of FE simulations, using a material model that is capable of accurately reproducing the deformation behavior of the material is necessary.

In the case of sheet metal forming simulation, biaxial tensile test and reverse loading test are most popular advanced testing method for considering the actual plastic deformation. Cruciform specimen is loaded for biaxial tensile stress and plastic deformation behavior is measured [2]. Using a yield function that is capable of accurately reproducing under the biaxial stress state is important for accurate FE simulation [3, 4]. Uniaxial tensile specimen is loaded for tension and compression stress and Bauschinger effect is measured in the reverse loading test. For accurate FE simulation, including the reverse loading state, using an accuracy hardening rule that is capable of accurately reproducing under reverse loading test is important [5]. However, previous research about these phenomena are investigated on limited stress and strain state such as an almost proportional or uniaxial stress state.

On the other hand, cold drawing [6], UOE pipe forming [7, 8], roll forming, tube bending, and straightening [9] are performed; pipe manufacturing and forming process are loaded under the multiaxial and reverse stress and strain state in axial, circumferential, and thickness direction. To improve the predictive accuracy for FE simulations, considering the material anisotropy and Bauschinger effect on cold working process on the pipes is necessary. However, very few studies exist on material modeling and verification under the multiaxial and reverse stress-strain state [10].

The objective of the present study is to clarify the effect of the reverse loading under the biaxial stress state and validate the accuracy of existing material models. An appropriate yield function for the test material was determined by multiaxial tube expansion test using tubular specimens. Nonlinear kinematic hardening parameter was determined by reverse loading test using small uniaxial tensile specimen. Then, combined biaxial stresses were loaded to the tubular specimens and the accuracy of nonlinear kinematic and isotropic hardening models was validated.

2 EXPERIMENTAL METHODS

Seamless, low-carbon-steel tube was chosen as the test material; as shown in **Figure 1(a)**, it was fabricated using a hot pipe making process. **Table 1** shows the chemical composition of the test material. Tubular and small uniaxial tensile specimens were made by machining from center of the mother tubes and used in the material tests. Small uniaxial tensile specimens were fabricated from the mother tube wall in the axial and circumferential directions. Initial anisotropy and SD effect were not observed in uniaxial tension and compression tests in both directions.

2.1 Multiaxial tube expansion test

Figure 2 shows schematic of the servo-controlled multiaxial tube expansion testing machine developed by Kuwabara and Sugawara [11]. By controlling axial forces and an internal hydraulic pressure, this testing apparatus is capable of applying arbitrary biaxial stress paths to the central section of the tubular specimen shown in Figure 1(b). An axial force T and internal pressure P were applied to a tubular specimen by a hydraulic cylinder and pressure booster, respectively. These were measured using a load cell and pressure gauge, respectively, and the variable ranges were $-200 \le T \le 200\text{kN}$ and $0 \le P \le 50\text{MPa}$.

Table 1: Chemical composition of the test material.

C	Si	Mn	P	S	Fe
0.21	0.19	0.5	0.18	0.03	Bal.

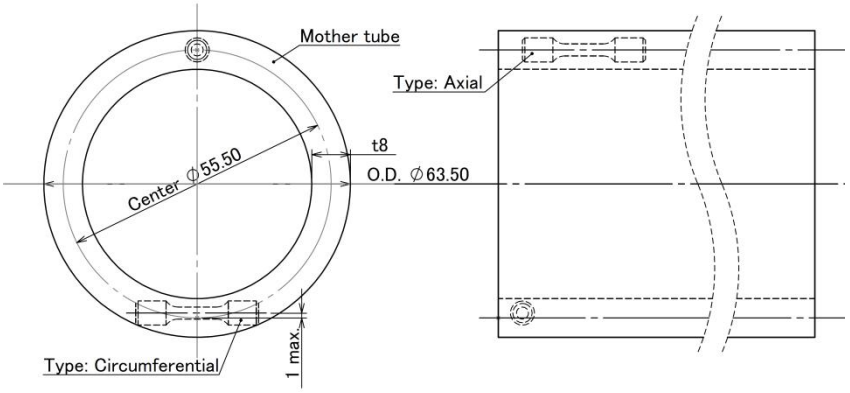

(a) Schematic of mother tube and cutting view of small uniaxial tensile specimen.

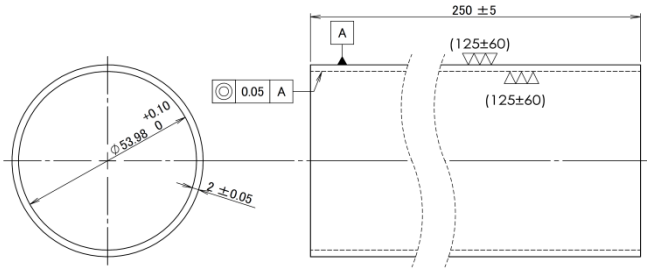

(b) Tubular specimen.

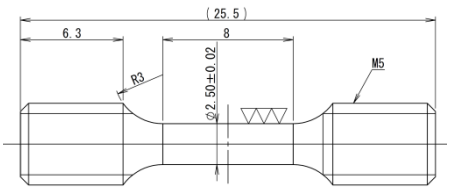

(c) Small uniaxial tensile specimen.

Figure 1: Schematic of mother tube and specimens.

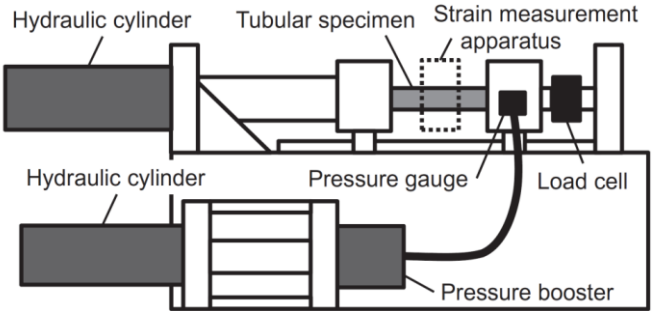

Figure 2: Schematic of the multiaxial tube expansion testing machine.

Axial and circumferential strains, ε_ϕ and ε_θ, and radius of axial curvature R_ϕ were measured continuously by 6 displacement transducers that are installed in the center of the testing machine. The axial and circumferential stresses, σ_ϕ and σ_θ, at the mid-section of the bulging specimen were calculated as the values at the mid wall using equations (4) and (5):

$$\sigma_\phi = \frac{P\pi(D/2-t)^2 + T}{\pi(D-t)t} \tag{4}$$

$$\sigma_\theta = \frac{(R_\phi - t)(D-2t)}{(2R_\phi - t)t} P - \frac{D-t}{2R_\phi - t}\sigma_\phi \tag{5}$$

based on the equilibrium requirements for a material element at the mid-section of a specimen.

2.2 Uniaxial reverse loading test

Uniaxial tension–compression reverse loading test was performed using a small uniaxial tensile specimen shown in Figure 1(c); it was preformed to quantitatively evaluate the Bauschinger effect of the test material. The specimen was fixed by screw on the ends. A stout frame around the specimen was used to prevent buckling.

2.3 Reverse loading tests under biaxial stress states

Compressive preloading (first loading) in the axial direction was applied by a hydraulic press machine to the mother tube. Consequently, tubular specimens were fabricated from the prestrained mother tube by machining. This was followed by the application of linear stress paths in the first quadrant of the principal stress space (second loading) to the prestrained tubular specimens for measuring the Bauschinger effect in the second loading.

3 RESULTS AND DISCUSSION

3.1 Multiaxial tube expansion test under liner stress paths

Tubular specimens were subjected to proportional loading with true stress ratios $\sigma_\phi : \sigma_\theta$ = 4:1, 2:1, 4:3, 1:1, 3:4, 1:2, and 1:4. The small uniaxial tensile specimens were used for uniaxial tensile tests with $\sigma_\phi : \sigma_\theta$ = 1:0 and 0:1.

Figure 3 shows representative example of true stress–true plastic strain curves (s–s curves) measured using the tubular specimens or small uniaxial tensile specimens (uniaxial stress

states). The s–s curves were successfully measured up to a strain level of specimen fracture for all stress ratios.

Figure 3(a) shows the results of $\sigma_\phi : \sigma_\theta$ = 1:0, i.e., a uniaxial s-s curve in axial direction that was in good agreement with Swift's power law. Figure 3(b) shows the results of $\sigma_\phi : \sigma_\theta$ = 4:1, the strain increment in θ – direction was minus because the stress state was close to uniaxial. Figure 3(c) shows the results of $\sigma_\phi : \sigma_\theta$ = 1:1; s–s curves overlapped with each other because the test material had initial isotropy. Figure 3(d) shows the results of $\sigma_\phi : \sigma_\theta$ = 1:2; the stress ratio gives the plane strain state, and thus, the plastic strain increment in the ϕ direction remains zero.

These results marshaled contours of plastic work [12, 13] in the stress space and they were used to quantitatively evaluate the work hardening behavior of the test material under biaxial tension. The s-s curve obtained from a uniaxial tensile test in the axial direction was selected as a reference datum for work hardening; the uniaxial tensile true stress σ_0 and the plastic work per unit volume W_0 associated with a particular value of offset true plastic strain $\varepsilon_0^{\mathrm{p}}$ were determined (**Figure 4(a)**). The uniaxial true stress σ_θ in the circumferential direction and the biaxial true stress components $(\sigma_\phi, \sigma_\theta)$ were then determined at the same plastic work as W_0 (equation (6) and Figure 4(b)). The stress points $(\sigma_0, 0)$, $(0, \sigma_\theta)$, and $(\sigma_\phi, \sigma_\theta)$ were plotted in the principal stress space form a contour of plastic work associated with a particular value of $\varepsilon_0^{\mathrm{p}}$ (Figure 4(c)). When $\varepsilon_0^{\mathrm{p}}$ is considered to be sufficiently small, the work contour

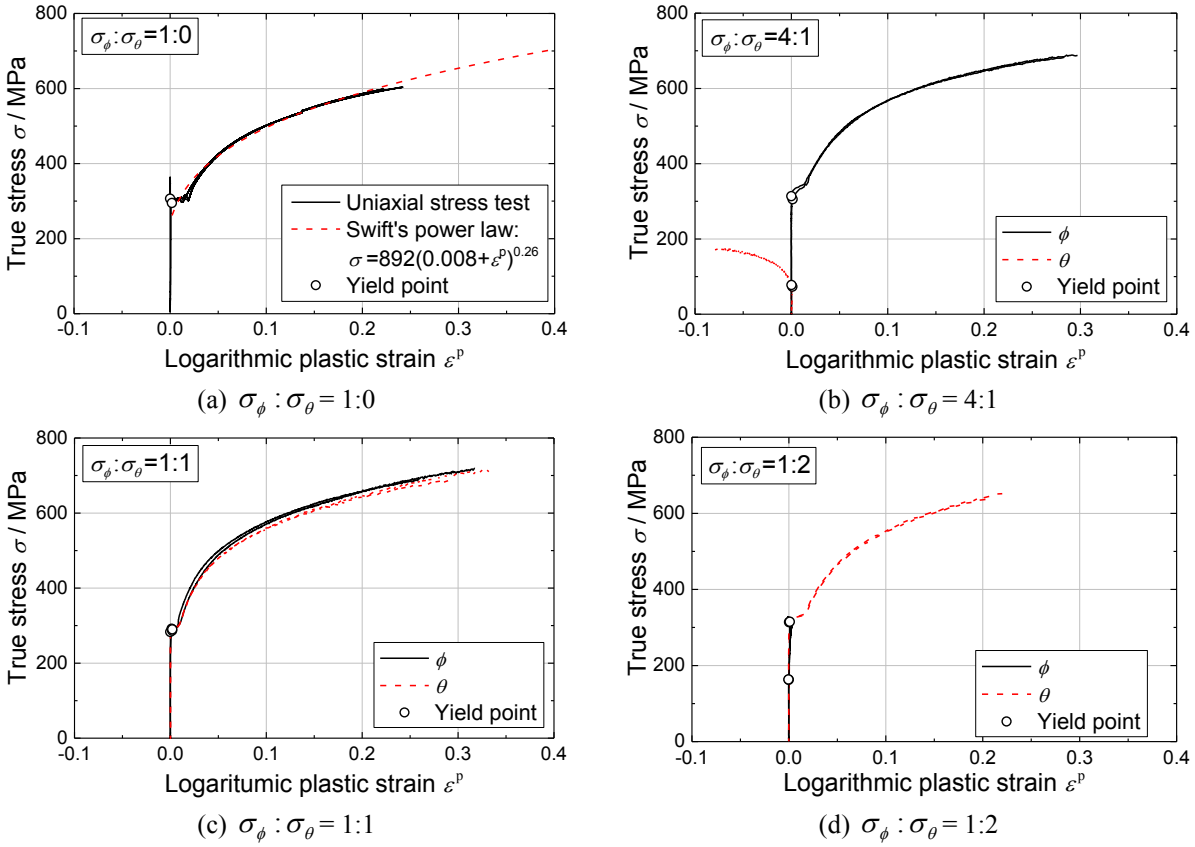

(a) $\sigma_\phi : \sigma_\theta$ = 1:0 (b) $\sigma_\phi : \sigma_\theta$ = 4:1

(c) $\sigma_\phi : \sigma_\theta$ = 1:1 (d) $\sigma_\phi : \sigma_\theta$ = 1:2

Figure 3: True stress-logarithmic plastic strain diagrams measured using multiaxial tube expansion tests with yield points.

$$W_0 = \int_0^{\varepsilon_0^{\mathrm{p}}} \sigma_\phi d\varepsilon_\phi \Big|_{\text{uniaxialtensilestate}} = W_\phi + W_\theta = \int_0^{\varepsilon_\phi^{\mathrm{p}}} \sigma_\phi d\varepsilon_\phi + \int_0^{\varepsilon_\theta^{\mathrm{p}}} \sigma_\theta d\varepsilon_\theta \tag{6}$$

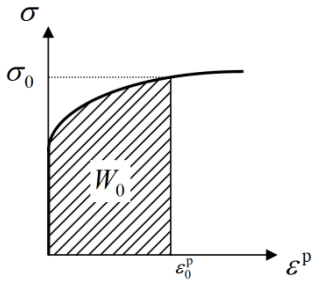

(a) True stress-logarithmic plastic strain curve in axial direction and associated plastic work W_0

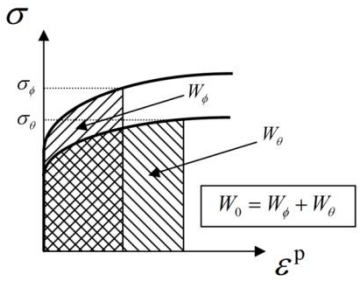

(b) Biaxial stress values at plastic work of W_0

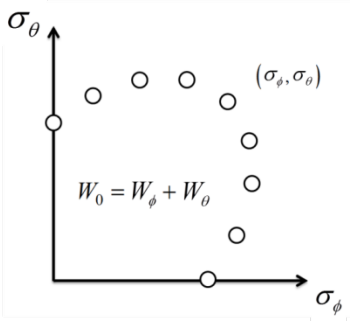

(c) Plotting each stress values in principle stress space

Figure 4: Calculation method of stress points at equal plastic work of W_0.

can be practically viewed as a yield locus.

Figure 5(a) shows measured stress points forming the contours of plastic work for different levels of $\varepsilon_0^{\mathrm{p}}$. The maximum value of $\varepsilon_0^{\mathrm{p}}$ for which the work contour has a full set of nine stress points was $\varepsilon_0^{\mathrm{p}} = 0.24$, which was limited by the maximum loading point in uniaxial tensile test in axial direction.

Figure 5(b) shows the stress points forming contours of plastic work, the values of which are normalized by σ_0 associated with $\varepsilon_0^{\mathrm{p}}$. The normalized stress points do not stay constant; the material exhibits "Differential hardening" (DH). However, the degree of DH is small.

The theoretical yield loci based on the von Mises [1], Hill's quadratic [14], and the Yld2000-2d [15] yield functions are superimposed in the figure. The unknown parameters of the Hill's quadratic yield function were determined using $\sigma_\phi, \sigma_\theta$, and σ_{b} and those of the Yld2000-2d yield function were determined using r_ϕ, r_θ, and r_{b} and $\sigma_\phi, \sigma_\theta$, and σ_{b}, where σ_{b} and r_{b} are the equal biaxial tensile flow stress $\sigma_\phi = \sigma_\theta = \sigma_{\mathrm{b}}$ and the ratio of the plastic strain increments $d\varepsilon_\theta^{\mathrm{p}} / d\varepsilon_\phi^{\mathrm{p}}$ at $\varepsilon_0^{\mathrm{p}}$=0.10, respectively, and r_α is the *r*-value in uniaxial tensile state at $\varepsilon_0^{\mathrm{p}}$=0.10. Then, r_ϕ, r_θ, and r_{b} are assumed 1 because of the test material having initial isotropy and because it is difficult to measure the *r*-value at uniaxial tensile state for the tubular material. The exponent of the Yld2000-2d yield function was assumed 6 because the test material is a b.c.c. material. The von Mises yield function overestimates the work

contours at all stress paths except at $\sigma_\phi : \sigma_\theta$=1:0 and 0:1. Hill's quadratic yield function overestimates the work contours in the vicinity of plane strain tension, i.e., $\sigma_\phi : \sigma_\theta$=2:1 and 1:2. The Yld2000-2d has a better agreement with the measured work contours.

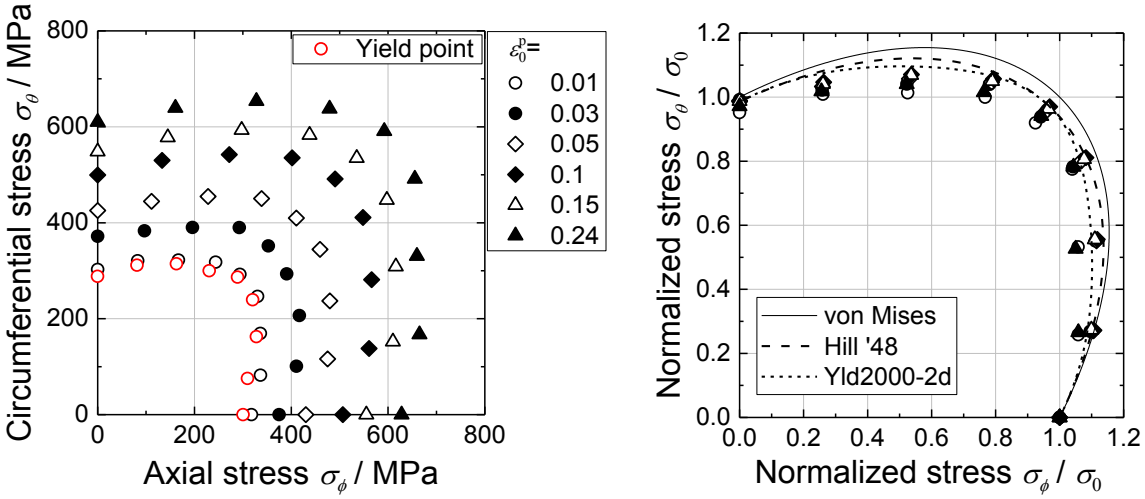

(a) Contours of plastic work.

(b) Normalized contours of plastic work and calculated theoretical yield loci.

Figure 5: Measured stress points forming contours of plastic work compared with theoretical yield loci.

3.2 Uniaxial reverse loading test

Uniaxial tension–compression reverse loading tests were performed using small uniaxial tensile specimens to quantitatively evaluate the Bauschinger effect of the test material. **Figure 6(a)** shows the results of a reverse loading test under the uniaxial stress state in axial direction and calculated curve using nonlinear kinematic hardening (NKH) model [16, 17] (equations (7–9)), and isotropic hardening (IH) model using Swift's power law with the von Mises yield function. The NKH ratio C uses two values: C_1 and C_2; in first loading $C = C_1$ and in the second loading $C = C_2$. Unknown parameters are identified to reproduce cyclic loading test using a least-square approach (approximated values are shown in **Table 2**). Here, C_1 is assumed to be 2000 to prevent C_1 rise up to infinity because of the test material shows yield point elongation (YPE) in the first loading. The experimental result is in good agreement with the NKH calculation. The IH model is inferior to the NKH model with respect to the reproducibility of the test material's Bauschinger effect.

Furthermore, Figure 6(b) shows the measured uniaxial stress–strain curve in axial direction and that calculated using the NKH model, the parameters of which are shown in Table 2; the experimental result is in good agreement with the NKH calculation again.

3.3 Biaxial tensile stress test after axial prestraining

Combined stress path experiments using prestraind tubular specimens were performed to investigate the effect of axial prestraining on the stress–strain curves in the second loading. **Figure 7** shows the stress paths in the first (prestraining) and second loading. **Figure 8** shows

$$f = \phi(\boldsymbol{\sigma} - \boldsymbol{\alpha}) - (Y_0 + R) \tag{7}$$

$$\boldsymbol{\alpha} = \boldsymbol{\alpha}_1 + \boldsymbol{\alpha}_2$$

$$d\boldsymbol{\alpha}_1 = C\left(a d\boldsymbol{\varepsilon}^{\mathrm{p}} - \boldsymbol{\alpha}_1 d\bar{\varepsilon}^{\mathrm{p}}\right) \tag{8}$$

$$d\boldsymbol{\alpha}_2 = H_\infty d\boldsymbol{\varepsilon}^{\mathrm{p}}$$

$$dR = b(Q - R)d\bar{\varepsilon}^{\mathrm{p}} \tag{9}$$

ϕ : Yield function

Y_0 : Yield stress

C : Nonlinear kinematic hardening ratio

a : Saturated value of nonlinear kinematic hardening

H_∞ : Linear kinematic hardening ratio

b : Isotropichardening ratio

Q : Saturated value of isotropichardening

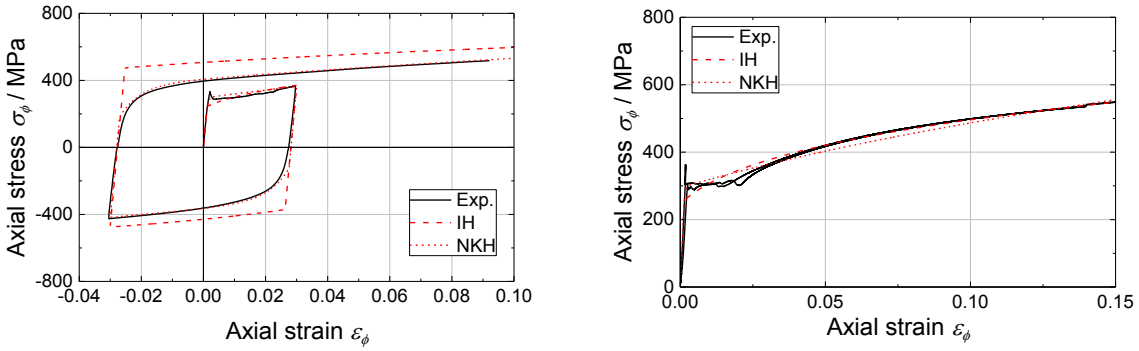

(a) Reverse loading test (b) Uniaxial tensile test

Figure 6: The result and calculation of reverse loading and tensile tests under the uniaxial stress state.

Table 2: Approximated parameters in NKH model.

Y_0/MPa	202.6
C_1/-	2000
C_2/-	156.3
a /MPa	94.6
H_∞/MPa	865.0
b /-	9.315
Q /MPa	173.1

the measured s–s curves and calculated s–s curves based on the NKH model and IH model. Here, the origin in x-axis ($\varepsilon_\phi, \varepsilon_\theta$) is shifted to zero to determine the effect of reloading.

Figure 8(a) shows uniaxial tensile state in axial direction on second loading, which is overestimated using IH. Using NKH calculation, re-yielding behavior and flow stress are shown to be in well agreement because parameter of NKH was approximated in uniaxial

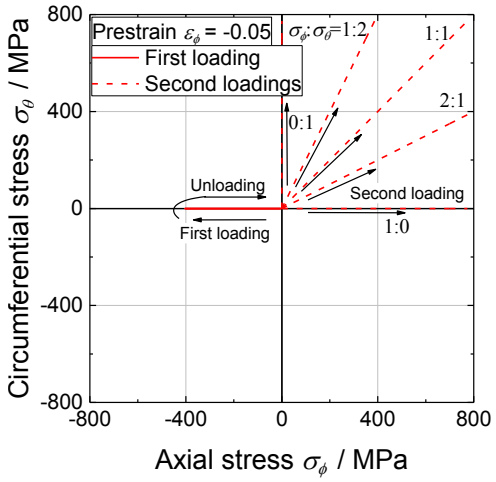

Figure 7: Loading path diagram of reverse loading test under the biaxial stress state.

stress state.

Figure 8(b) shows the results of $\sigma_\phi : \sigma_\theta$ = 2:1; re-yielding behavior is shown to be in agreement using NKH; however, the flow stress is calculated to be lower than the experimental. Strain increment in θ direction is calculated $d\varepsilon_\theta = 0$ using IH; however, the NKH calculation and the experimental result indicate $d\varepsilon_\theta < 0$; this is because the outward normal vector of the yield function at $\sigma_\phi : \sigma_\theta$ = 2:1 is negative in θ direction because of kinematic hardening caused by prestraining. These corroborate the validity of the associated flow rule on reverse loading under biaxial stress state.

Figure 8(c) shows the results of $\sigma_\phi : \sigma_\theta$ = 1:1; strain increment ratio around re-yielding becomes $d\varepsilon_\theta < d\varepsilon_\phi$ because of the same reason of previous consideration; these validate the NKH model. However, flow stress is calculated to be lower than the experimental.

Figure 8(d) shows the results of $\sigma_\phi : \sigma_\theta$ = 1:2. The experimental result shows $d\varepsilon_\phi > 0$, which is different from the experimental $\sigma_\phi : \sigma_\theta$ = 2:1 in the minimum principal stress direction because of the same reason of previous consideration; these are shown using NKH.

Figure 8(e) shows the results of $\sigma_\phi : \sigma_\theta$ = 0:1; the stress state in second loading is changed to 90° from the first loading in stress space. The flow stress is shown to be reproduced using IH, and the effect of first loading is limited to only the early phase after re-yielding.

4 CONCLUSIONS

Reverse loading tests under the uniaxial and biaxial stress states were performed using seamless carbon steel tubes. The conclusions of this study are summarized as follows:

- The test material exhibited differential hardening behavior under proportional loading. The Yld2000-2d yield function with an exponent of 6 could reproduce the initial and successive contours of plastic work in the principal stress space (Figure 5).
- The experimental results were in good agreement with the prediction by the NKH model under the uniaxial tension–compression reverse loading (Figure 6(a) and Figure 8(a)).
- Reverse loading tests (axial compression followed by biaxial tension) were performed using the multiaxial tube expansion testing method. The observed strain

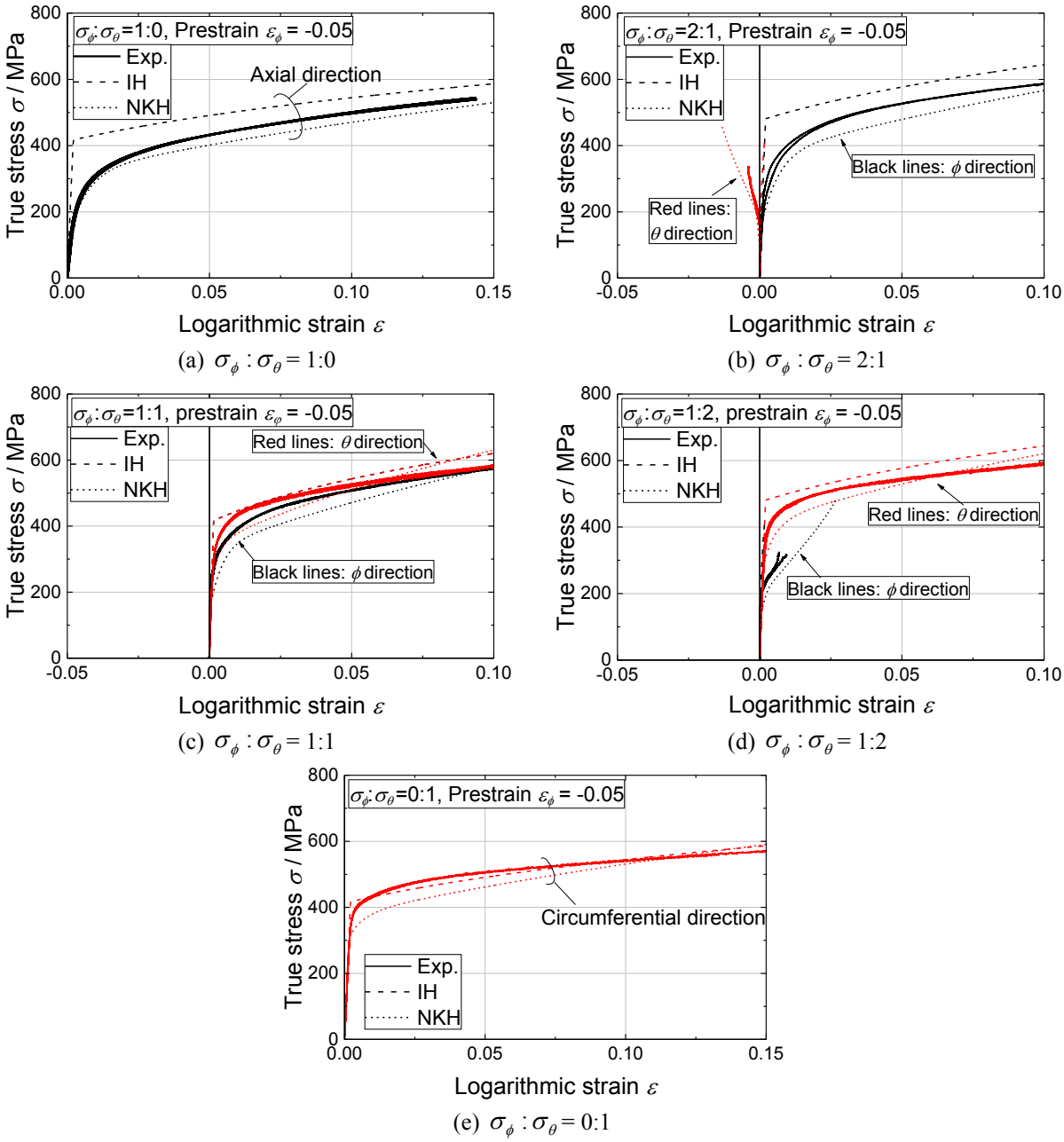

Figure 8: The experimental result compared with the calculated under the biaxial reverse loading state.

increments were in qualitative agreement with those predicted using the NKH model. However, the flow stresses were not well reproduced by the NKH model (Figure 8).

- In order to improve the predictive accuracy of the FEA for cold working processes on steel tubes, it is necessary to perform material testing for not only limited stress states, such as proportional loading and reverse loading under uniaxial stress states, but also for more complex stress states using the multiaxial tube expansion testing method.

REFERENCES

[1] Von Mises, R. Mechanik der festen Korper un plastich deformablen Zustant. Göttingen Nachrichten. *Math.-Phys. Klasse* (1913): 582–592.

[2] Kuwabara, T. Ikeda, S. and Kuroda, T. Measurement and analysis of differential work-hardening in cold-rolled steel sheet under biaxial tension. *J. Mater. Process Technol*. (1998) **80**-81: 517-523.

[3] Kuwabara, T. Hashimoto, K. Iizuka, E. and Yoon, J.W. Effect of anisotropic yield functions on the accuracy of hole expansion simulations. *J. Mater. Process. Technol.* (2011) **211**: 475-481.

[4] Yanaga, D. Kuwabara, T. Uema, N. and Asano, M. Material modeling of 6000 series aluminum alloy sheets with different density cube textures and effect on the accuracy of finite element simulation. *Int. J. Solids Struct*. (2012) **49**: 3488–3495.

[5] Yoshida, F. and Uemor, T. A model of large-strain cyclic plasticity and its application to springback simulation. *Int. J. Mech. Sci.* (2003) **45**: 1687–1702.

[6] Sawamiphakdi, K. Lahoti, G. D. and Kropp, P. K. Simulation of a tube drawing process by the finite element method. *J. Mater. Process. Technol*. (1991), **27**: 179–190.

[7] Herynk, M.D. Kyriakides, S. Onoufriou, A. Yun, H.D. Effects of the UOE/UOC pipe manufacturing processes on pipe collapse pressure. *Int. J. Mech. Sci.* (2007) **49**: 533–553.

[8] Tsuru, E. and Agata, J. Forming and buckling simulation on high-strength UOE pipe with plastic anisotropy. *NSC Technical Report* (2013) **102**: 70-78.

[9] Kasai, T. Takasu, I. Research on reduction of residual stress on bearing steel tubes. *Sanyo Technical Report* (2004) **11**: 33-40.

[10] Ohashi, Y. Kawashima, K. and Yokochi, T. Anisotropy due to plastic deformation of initially isotropic mild steel and its analytical formulation. *J. Mech. Phys. Solids*. (1975) **23**: 277-294.

[11] Kuwabara, T. and Sugawara, F. Multiaxial tube expansion test method for measurement of sheet metal deformation behavior under biaxial tension for a large strain range. *Int. J. Plast*. (2013) **45**: 103-118.

[12] Hill, R. and Hutchinson, J.W. Differential hardening in sheet metal under biaxial loading: a theoretical framework. *J. Appl. Mech.* (1992) **59**: S1-S9.

[13] Hill, R. Hecker, S.S. and Stout, M.G. An investigation of plastic flow and differential work hardening in orthotropic brass tubes under fluid pressure and axial load. *Int. J. Solids Struct*. (1994) **31**: 2999-3021.

[14] Hill, R. A theory of the yielding and plastic flow of anisotropic metals. *Proc. Roy. Soc. London* (1948) **A193**-1033: 281–297.

[15] Barlat, F. Brem, J.C. Yoon, J.W. Chung, K. Dick, R.E. Lege, D.J. Pourboghrat, F. Choi, S.H. and Chu, E. Plane stress yield function for aluminum alloy sheets – Part I: Theory. *Int. J. Plast*. (2003) **19**: 1297–1319.

[16] Armstrong, P.J. and Frederick, C.O. A mathematical representation of the multiaxial Bauschinger effect. *C.E.G.B. Report* RD/B/N (1966) **731**.

[17] Chaboche, J.L. and Rousselier, G. On the plastic and viscoplastic constitutive equations-part I: Rules developed with internal variable concept. *J. Press. Vessel Technol*. (1983) **105**: 153-158.